Chapter 5: Design and Simulation Studies of Gyrotron Using Multi-Section Slightly tapered RF Cavity

5.1 Introduction

In the preceding Chapter – 4, the PBG cavity has been used in place of the straight section of the three-section RF interaction cavity of the gyrotron. The design, PIC simulation, and Multimode simulation of PBG cavity-based gyrotron have been investigated to observe the gyrotron's transient behavior. The magnetic tuning scheme has been used to obtain the tuneable bandwidth of the PBG gyrotron for DNP / NMR applications. The use of the PBG cavity reduces the mode competition in the cavity, increasing the tunable bandwidth of the gyrotron. The operation of these gyrotrons is limited due to their cylindrical RF circuit because the start oscillation current (SOC) of these gyrotrons is tremendously increased at higher-order axial modes (HOAMs) of operation. This leads to severe mode competition between the axial modes and their next higher-order mode in the cavity. The SOC of the cavity is directly proportional to the product $L_{eff}^{2} Q_{T}^{-1}$, where, L_{eff} and Q_T are the effective cavity length and total quality factor, respectively, and $Q_T = Q_d / \left(1 + Q_d Q_{ohm}^{-1}\right)$ [128] – [129]. The Q_T is decreasing with the diffractive quality factor (Q_d). For HOAMs of operation in conventional gyrotron cavities, the effective cavity length (L_{eff}) [130] increases by a very small amount but the diffractive quality factor (Q_d) decreases dozens of times because Q_d is proportional to q^{-2} [129]. Therefore, the RF cavity operation in HOAMs increases the SOC, which in turn promotes the mode competition. The diffractive quality factor can be maintained remarkably by modifying the cavity even when operating in HOAMs [131] – [132]. The three-section cavity modification [112] is done by adding a slightly tapered section at either end of the straight section and slightly tapering the straight section. Thus, the SOC does not increase much and the mode competition reduces even in HOAMs

operation in the multi-section cavity, which helps to enhance the tuneable bandwidth of the gyrotron.

In the present chapter, the millimeter-wave gyrotron's tuneable bandwidth has been enhanced by modifying the three-section cavity into a multi-section cavity. The continuous tuning of the present multi-section RF cavity gyrotron is obtained using magnetic tuning schemes. The rest of the chapter has been organized as follows. The design and analysis of the multi-section cavity have been described in section 5.2. PIC simulation of multi-section cavity gyrotron has been described in section 5.3 and section 5.4 thermal and structural analyses have been presented. The tuneability of the present millimeter wave gyrotron has been described in section 5.5. The discussion on fabrication error has been given in section 5.6 and the conclusion has been made in section 5.7.

5.2 Design of Multi-Section Cavity

A multi-section cavity is designed by adding a slightly tapered section (L_2, θ_2 and L_4, θ_4) at either end of the uniform section of the three-section cavity and by slightly tapering (θ_3) the uniform section of the conventional cylindrical gyrotron cavity operating in $TE_{7,2}$ mode at 260 GHz [64], [112]. The design parameters (L_2, θ_2, L_4, θ_4, and θ_3) of the multi-section cavity are optimized by observing their effect on the resonating frequency (ω_r), and diffractive Q factor (Q_d).

5.2.1 Diffractive Quality Factor and Resonating Frequency

To achieve the maximum beam-wave interaction in the RF interaction cavity, the design parameters are chosen in such a way that the cavity field profile should be

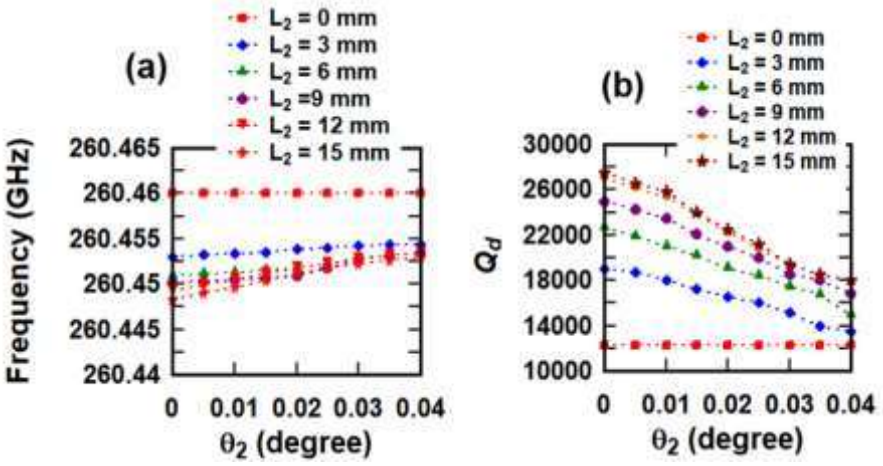

Figure 5.1 (a) Resonant frequency *Vs* taper angle θ_2, and (b) diffractive Q factor *Vs* taper angle θ_2 for different taper length L_2 of $TE_{7,2,1}$ mode [for $L_4 = 0$, $\theta_4 = 0$, $\theta_3 = 0$, $L_1 = 10$ mm, $L_3 = 22$ mm, $L_5 = 10$ mm, and $L_6 = 63$ mm].

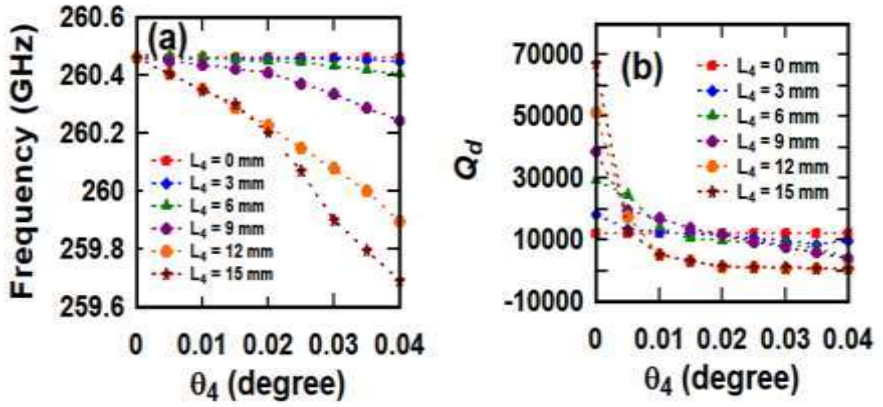

Figure 5.2 (a) Resonant frequency Vs taper angle θ_4, and (b) diffractive Q factor Vs taper angle θ_4 for different taper length L_4 of $TE_{7,2,1}$ mode [for $L_2 = 0$, $\theta_2 = 0$, $\theta_3 = 0$, $L_1 = 10$ mm, $L_3 = 22$ mm, $L_5 = 10$ mm, and $L_6 = 63$ mm].

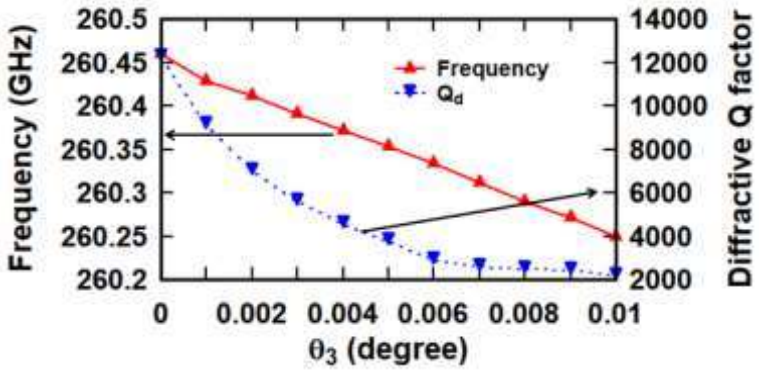

Figure 5.3 Resonant frequency and diffractive Q factor Q_d Vs taper angle θ_3 of $TE_{7,2,1}$ mode [for $L_2 = 0$, $\theta_2 = 0$, $L_4 = 0$, $\theta_4 = 0$, $L_1 = 10$ mm, $L_3 = 22$ mm, $L_5 = 10$ mm, and $L_6 = 63$ mm].

maximum at the mid of the cavity and smooth in the taper section. The cavity field profile of the cavity in the absence of the electron beam is obtained by using (2.86) and (2.87). The complex frequency is given as $\omega = 2\pi f_0 \left(1 + j/2Q_d\right)$, where, f_o is the operating frequency, and Q_d is the diffractive quality factor, which satisfies (2.86). There is no direct method available to calculate the resonating frequency (ω_r) and the diffractive quality factor (Q_d) of the cavity using (2.86) and (2.87) for the multi-section slightly tapred cavity. Therefore, in the present case, the minimization method is used to estimate the combination of ω_r and Q_d by minimizing the value of (2.87) at z = z_{out} as much as possible [133]. To estimate the ω_r and Q_d, the objective function F(x) is minimized, which is defined as

$$F(x) = \left| \frac{df(\mathrm{x})}{dz} + i\,k_z(\mathrm{x})\,\mathrm{f(x)} \right|_{z = z_{out}} \tag{5.1}$$

where, 'x' is a vector of two-real value design variables ω_r and Q_d. The golden search technique [134] is used to find the minimum value of function *F(x)* in the cyclic coordinate search method [135]. In this method, one variable is changed at a time while the other one is fixed. The obtained combination of ω_r and Q_d has been carried out again in the golden search section. Cyclic search for ω_r and Q_d is performed until the boundary condition (2.87) for $z = z_{out}$ is satisfied or the change in the value of both design variables from one cycle to another is reduced to a pre-defined tolerance limit ($\epsilon = 10^{-5}$). The estimated Q_d and ω_r are used as a reference to optimize the cavity field profile of the present multi-section cavity, which should be smooth in the tapered section. The effects of slightly tapered sections (L_2, L_3, and L_4) on Q_d and ω_r of the RF cavity are observed for $TE_{7,2,1}$ mode. The variation of L_2 and θ_2 do not have any significant effect on ω_r but does significantly affect Q_d, as shown in Figures 5.1 (a) and

Table 5.1: Structural Parameters of Multi-Section RF Cavity

R_1	1.85 mm	θ_1	3^0	L_1	10 mm
R_2	2.365 mm	θ_2	0.02^0	L_2	12 mm
R_3	2.369 mm	θ_3	0.007^0	L_3	22 mm
R_4	2.3717 mm	θ_4	0.01^0	L_4	12 mm
R_5	2.374 mm	θ_5	1^0	L_5	10 mm
R_6	2.55 mm	θ_6	2.24^0	L_6	63 mm
R_7	5 mm				

Table 5.2: Resonant Frequency, Quality Factors, Effective Length, and Frequency of the Multi-Section RF Cavity

q	f_r (GHz)	L_{eff} (mm)	Q_d	Q_{ohm}	Q_T	$f_r - f_r/Q_T$ (GHz)	$f_r + f_r/Q_T$ (GHz)
1	260.05	17.2	4900	9137	3190	259.97	260.13
2	260.29	28.5	5600	9140	3473	260.21	260.36
3	260.43	36.5	5200	9143	3315	260.35	260.51
4	260.59	40.1	3900	9146	2734	260.49	260.69
5	260.77	42.7	3000	9149	2259	260.66	260.89
6	261.01	45.0	2450	9153	1933	260.86	261.14
7	261.21	45.8	1900	9156	1573	261.04	261.38
8	261.48	46.2	1500	9161	1289	261.28	261.68
9	261.85	46.4	1200	9167	1061	261.55	262.05

5.1 (b), respectively. Figure 5.1 (a) predicts that ω_r increases as θ_2 increases for a fixed value of L_2 and ω_r decreases as L_2 increases for a particular value of θ_2. However, Q_d increases as L_2 increases for a particular value of θ_2 and Q_d decreases as θ_2 increases for a fixed value of L_2, as shown in Figure 5.1 (b). It means that the main role of L_2 section is to increase the effective length of the cavity and the Q_d, especially for HOAMs. The variation of L_4 and θ_4 significantly affect both the resonant frequency and the diffractive Q factor, as shown in Figures 5.2 (a) and 5.2 (b). Figure 5.2 (a) predicts that ω_r decreases as L_4 increases for a fixed value of θ_4 and and vice-versa. However, Q_d increases as L_4 increases for a fixed value of θ_4, and Q_d decreases as θ_4 increases for a fixed value of L_4, as shown in Figure 5.2 (b). For a small value of θ_4, the frequency ω_r decreases very modestly as L_4 increases. It means that L_4 plays a role in increasing the effective length of the cavity for a smaller value of θ_4. For a larger value of θ_4, L_4 plays a role to reduce the Q_d. Similarly, it is also observed that both ω_r and Q_d are decreased,

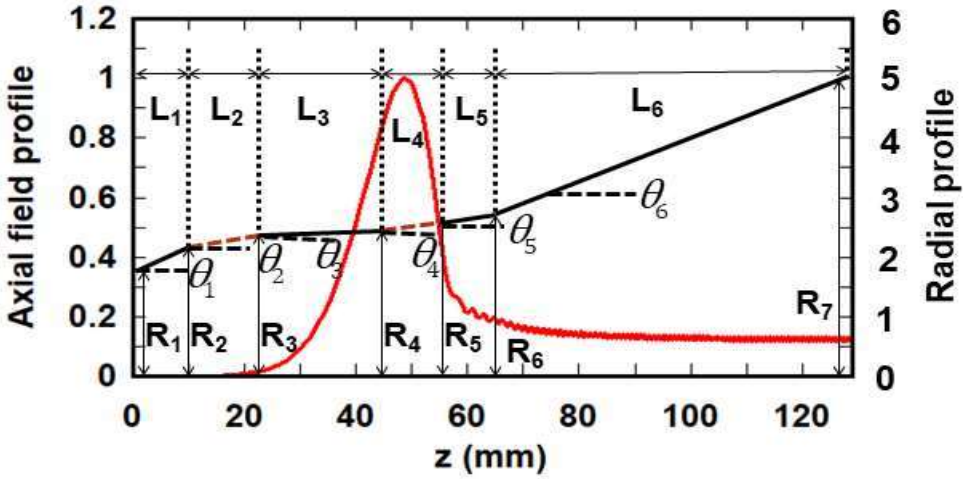

Figure 5.4 Cavity field profile and radial profile of the multi-section cavity.

as θ_3 is increased [Figure 5.3]. This effect is much higher at the lower order axial mode of operation than the HOAMs of operation in the RF cavity.

5.2.2 Cavity Field Profile

The optimized field profile for q = 1 and the cavity's radial profile are shown in Figure 5.4. The Q_d and ω_r are also estimated for the HOAMs. The cavity field profiles for different axial mode numbers, q = 1 – 9 [Figure 5.4 and Figures 5.5 (a) – 5.5 (h)] show that as the cavity field profile is shifted towards the low-frequency side (right) for q = 1 at which the cavity radius becomes slightly higher and while shifted towards the higher frequency side (left) for $q \geq 2$ at which the cavity radius becomes slightly lower. After observing the effect of design parameters on the ω_r, and Q_d, the multi-section cavity's design parameters are optimized. The structural parameters of the present multi-section RF interaction cavity are given in Table – 5.1. Due to the taper angles 0.02^o, 0.007^o and the shifting of the radius in section L_2, L_3, and L_4, it is calculated as ~4.19 µm, ~2.68 µm, and ~2.09 µm, respectively. This is within the fabrication limit of the cylindrical cavity made by copper material [95]. It is observed from Table – 5.2 that the Q_d is maintained a remarkable value even at HOAMs of operation of the RF cavity. This value is good enough for enhancing the tuneable

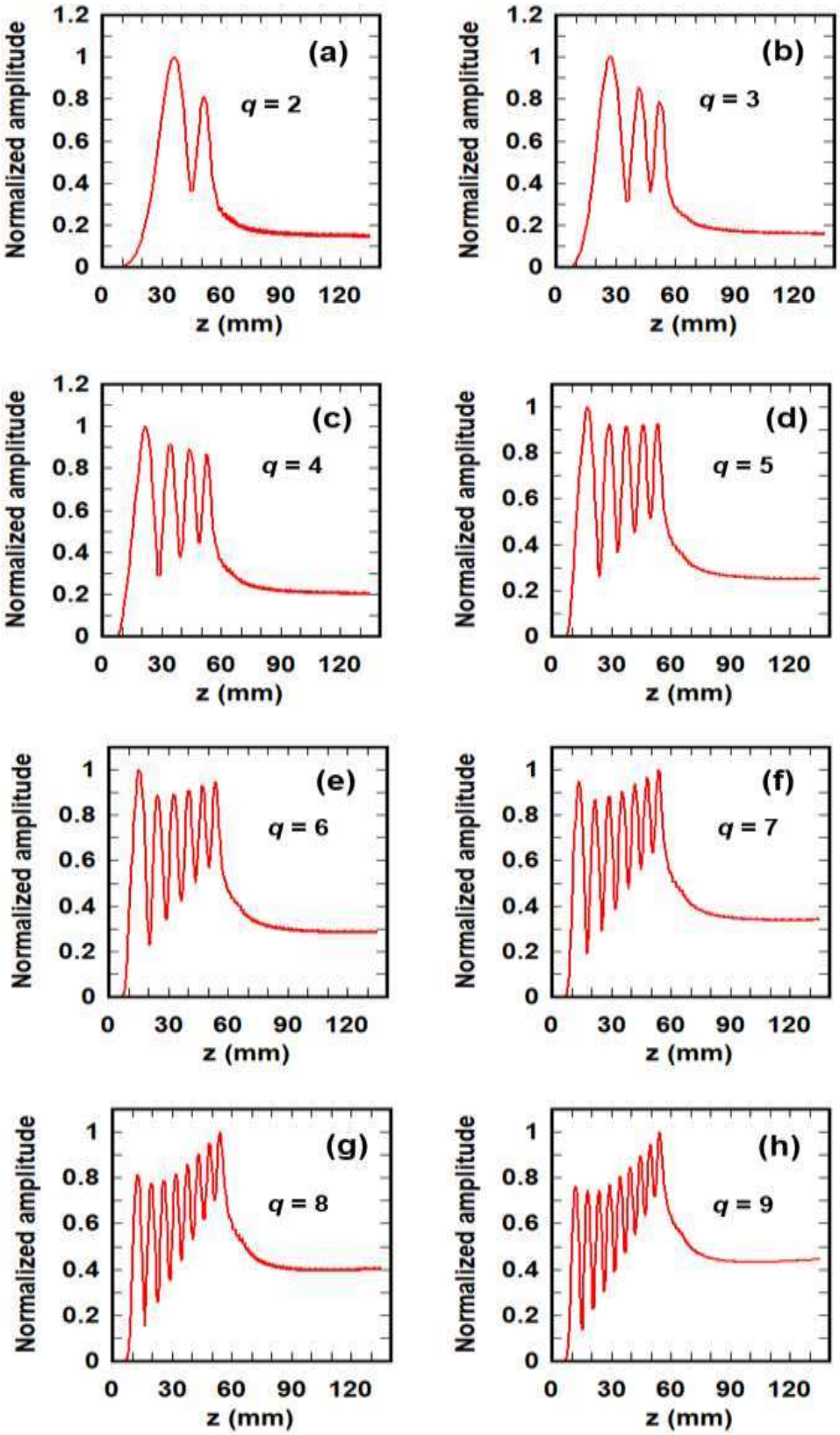

Figure 5.5 Cavity field profile for $TE_{7,2,q}$ mode (a) q = 2, (b) q = 3, (c) q = 4, (d) q = 5, (e) q = 6, (f) q = 7, (g) q = 8, and (e) q = 9.

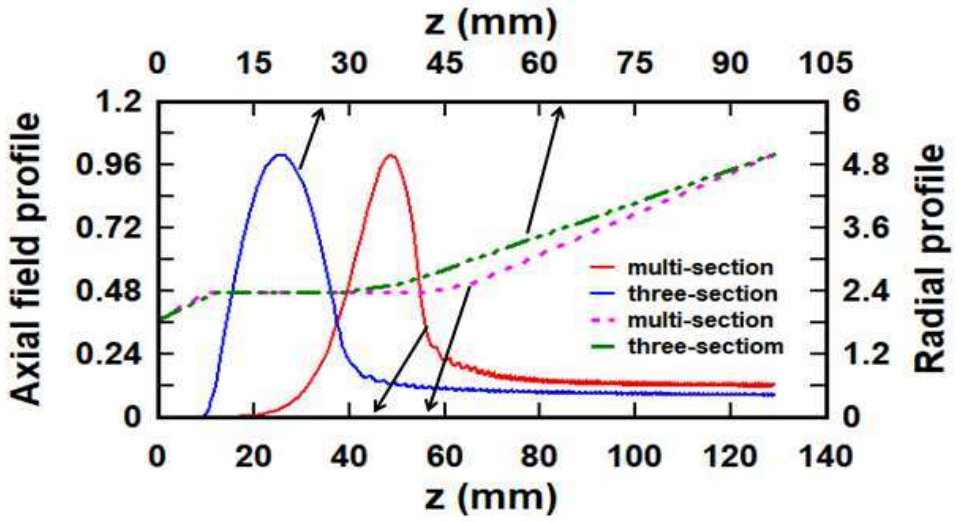

Figure 5.6 Comparison of the cavity field profile between the three-section cavity and multi-section cavity.

bandwidth of gyrotron. The cavity field profile (q = 1) of the multi-section cavity is compared to the three-section cavity [Figure 5.6] and found that the field profile of the multi-section cavity is shifted to the lower frequency side (right). The cavity field profile of the multi-section cavity without θ_2, θ_3, and θ_4 (L_2 = 12 mm, L_3 = 12 mm, θ_2 = θ_3 = θ_4 = 0^0) are also plotted for q = 1 – 9, as shown in Figures 5.7 (a) – 5.7 (i). The resonating frequency, effective length, and quality factors with respective the axial mode number q are given in Table – 5.3. It is observed that the frequency range (260.40 – 261.89 GHz) of the cavity without θ_2, θ_3, and θ_4 are less than the frequency range (260.05 – 261.85 GHz) of the multi-section cavity for q = 1 – 9. This happens because the cavity field profile of the cavity without θ_2, θ_3, and θ_4 have laid in constant radius but the cavity field profile of the multi-section cavity shifted right and left with respective axial mode number q.

5.2.3 Effective Length, Total Quality Factor and Start Oscillation Current

The effective length of the cavity can be given as [129] – [130],

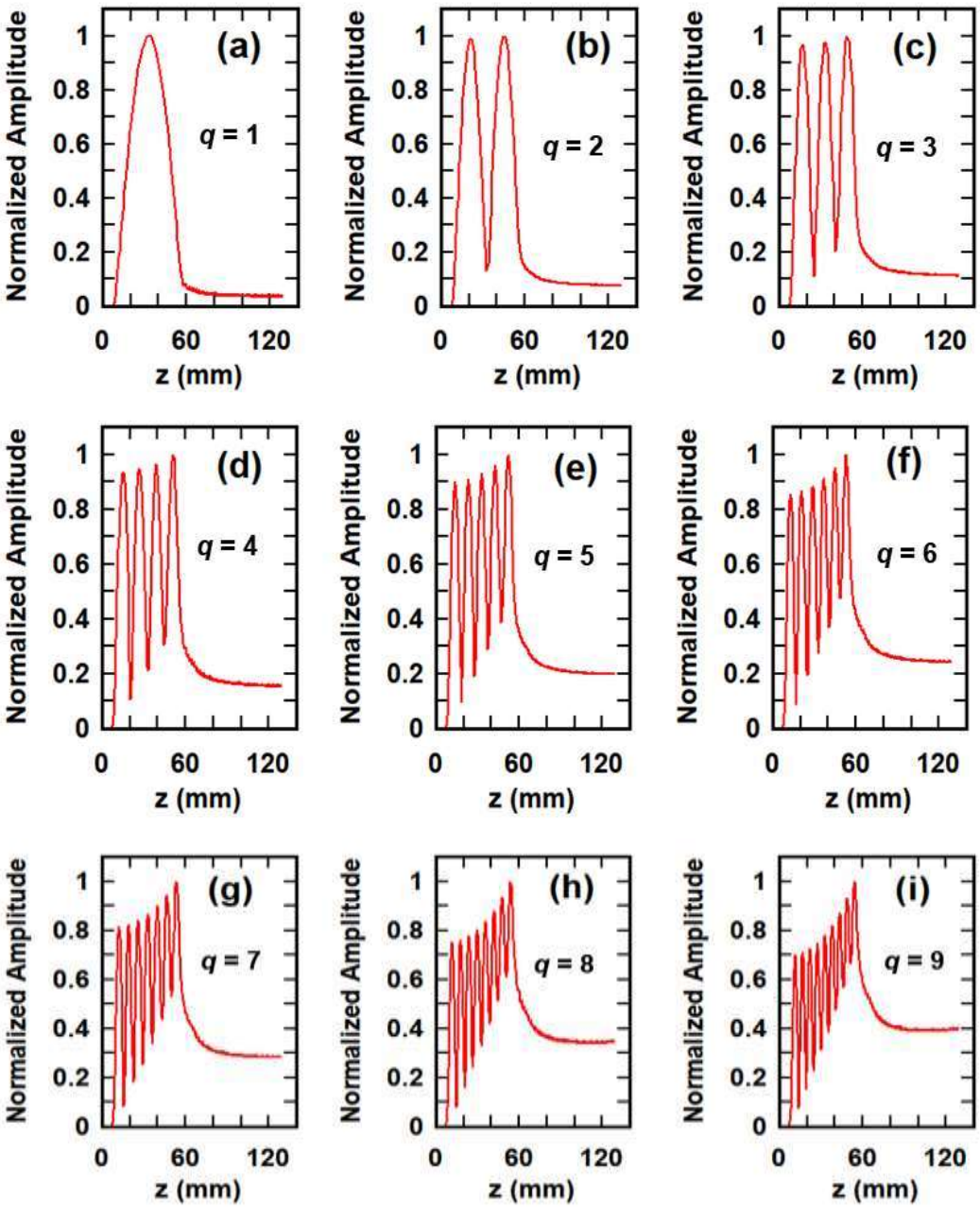

Figure 5.7 Cavity field profile for (a) $q = 1$, (b) $q = 2$, (c) $q = 3$, (d) $q = 4$, (e) $q = 5$, (f) $q = 6$, (g) $q = 7$, (h) $q = 8$, and (i) $q = 9$ [for $\theta_2 = 0$, $\theta_3 = 0$, $\theta_4 = 0$, $L_2 = 12$ mm, $L_4 = 12$ mm, $L_1 = 10$ mm, $L_3 = 22$ mm, $L_5 = 10$ mm, and $L_6 = 63$ mm].

$$L_{eff} \cong \left[0.075 \quad Q_d \; q^2 \lambda^3 \left(\frac{\chi_{m,n}}{\tan \theta} \right)^{1/3} \right]^{1/3} \tag{5.2}$$

Table 5.3: Resonant Frequency, Quality Factors, and Effective Length of the RF Cavity (For $\theta_2 = \theta_3 = \theta_4 = 0^0$, $L_2 = L_4 = 12$ mm)

q	f_r (GHz)	L_{eff} (mm)	Q_d	Q_{ohm}	Q_T
1	260.40	47.64	104200	9142	8405
2	260.47	47.63	26050	9143	6768
3	260.55	47.62	11577	9145	5109
4	260.68	47.60	6512	9147	3804
5	260.80	47.58	4168	9150	2864
6	261.04	47.56	2894	9154	2199
7	261.26	47.53	2126	9158	1726
8	261.52	47.49	1628	9163	1382
9	261.89	47.46	1286	9168	1128

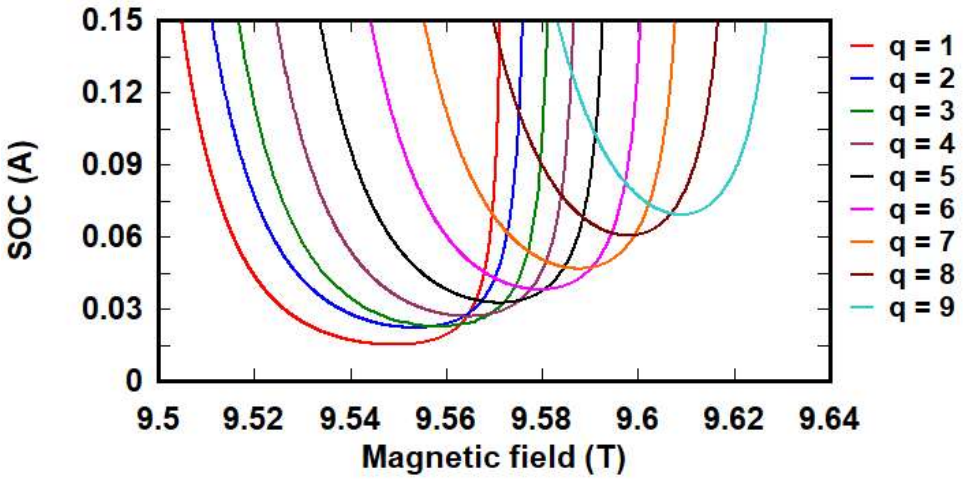

Figure 5.8 SOC for the $TE_{7,2,q}$ mode (q = 1 – 9).

where, λ is the operating wavelength and θ is the up-taper angle. The effective length (L_{eff}) of the cavity is calculated for the axial mode number, q = 1 to 9 using the corresponding diffractive quality factors mentioned in Table – 5.2. During the optimization of the cavity field profile, it is observed that for small values of θ_2 and θ_4, L_{eff} increases with respect to L_2 and L_4, respectively. As a result, Qd of the cavity increases, particularly for the HOAMs of operation [Table – 5.2]. Further, the diffractive quality factor (Q_d) is calculated by considering the cavity's effective length. The ohmic Q-factor (Q_{ohm}) is calculated by using $Q_{ohm} = (R/\delta)\left(1-\left(m^2/\chi_{mn}^2\right)\right)$ [1]. The total quality factor (Q_T) is calculated using both the obtained Q_{ohm} and Q_d of the present multi-section RF cavity [Table – 5.2]. The SOC [102] is calculated for the axial mode

Table 5.4: Design and Simulation Parameters of Multi-Section Gyrotron

Electrical Parameters	Voltage	15.5 kV
	Current	0.1 A
	Frequency	259.58 – 261.90 GHz
	Pitch factor	≤ 1.8
	Magnetic field	9.48 – 9.74 T
	Beamwidth	0.066 mm
	Beam radius	1.374 mm
	Velocity spread	~2 %
	Output power	1.5 – 114 W

number, q = 1 to 9 (Figure 5.8) by considering the corresponding total quality factors (Q_T), effective length of the cavity and operating frequency. The minimum SOC for the multi-section cavity is observed to be much lower than the minimum SOC of the conventional cylindrical gyrotron cavity in the respective axial mode number for $q \geq 2$. This is even more pronounced for the HOAMs of operation. The reduction in SOC proves to be very useful for preventing both mode competitions between different axial modes and nonstationary oscillations in the multi-section RF cavity [128].

5.3 PIC Simulation of Multi-Section Cavity Gyrotron

The present multi-section RF cavity is modeled using a Finite Integration Technique (FIT) based commercially available 3D simulation tool in "CST Particle Studio". Annealed copper is used to model the cavity with reduced conductivity, $\sigma = \sigma_{Cu}/2 = 2.9 \times 10^7$ S/ m. The PIC simulation descriptions and the phenomenon of phase bunching and beam-wave interaction process have already been explained in detail in Chapter – 3. The considered beam parameters in the PIC simulation are listed in Table – 5.4. After the beam wave interaction process, the RF signal developed at the output port in the desired operating $TE_{7,2,1}$ mode is observed as ~10.7 V. A neglibigible amount of Rf signal developed in competing modes such as $TE_{4,3}$ and $TE_{2,4}$, as shown in Figure 5.9 (a). The PIC simulation of a multi-section cavity-based gyrotron generates a continuous peak power ~ 114W in the $TE_{7,2,1}$ mode [Figure 5.9 (b)] and a meare amount of power

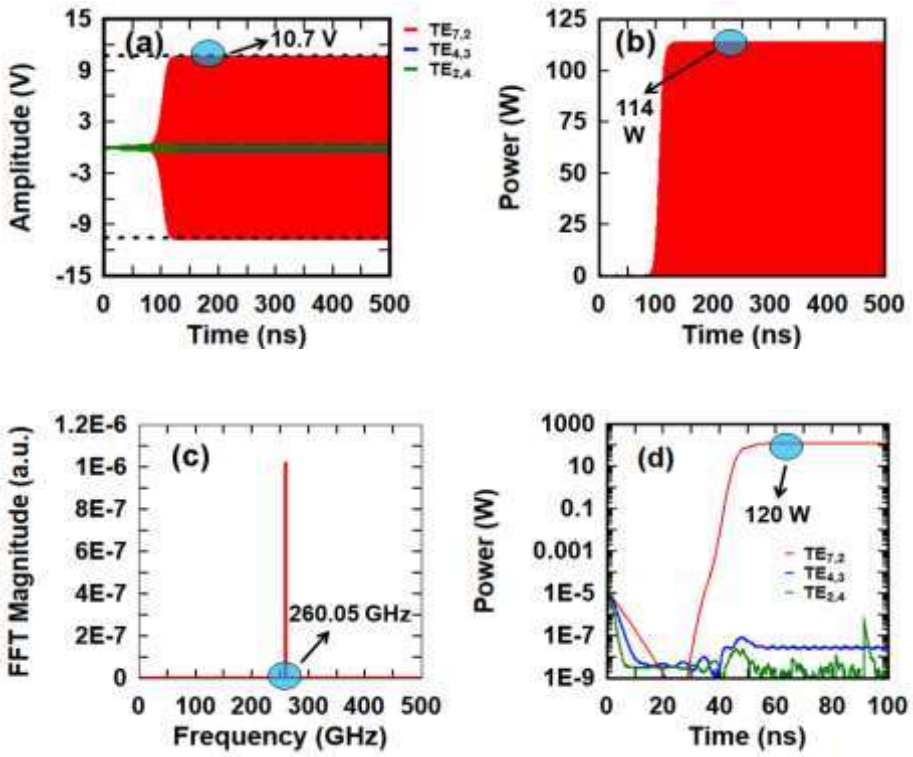

Figure 5.9 (a) Amplitudes of port signals (b) power in $TE_{7,2}$ mode (c) frequency spectrum of the port signal of $TE_{7,2}$ mode (d) output power through Multimode time-dependent calculation. The beam parameters 15.5kV, 100 mA, and α = 1.12 with a 2% velocity spread are considered in the PIC simulation and Multimode simulation.

in other competing modes such as $TE_{4,3}$ and $TE_{2,4}$. The resonating frequency is calculated as ~260.05 GHz [Figure 5.9 (c)] after taking the Fourier transform of generated signal in $TE_{7,2,1}$ mode. The obtained PIC simulation results are validated using a nonlinear time-dependent self-consistent Multimode code [91]. The Multimode code has predicted an RF power ~120 W [Figure 5.9 (d)] in $TE_{7,2,1}$ mode at 260.05 GHz for the same electron beam parameters as used in PIC simulation. The present PIC and multi-mode simulations are found to be in close agreement by ~5 %.

5.4. Thermal and Static Structural Analysis

The present multi-section cavity is modeled by using Finite Element Method (FEM) based simulation tool ANSYS [96]. The OFHC-Cu is used to model the present

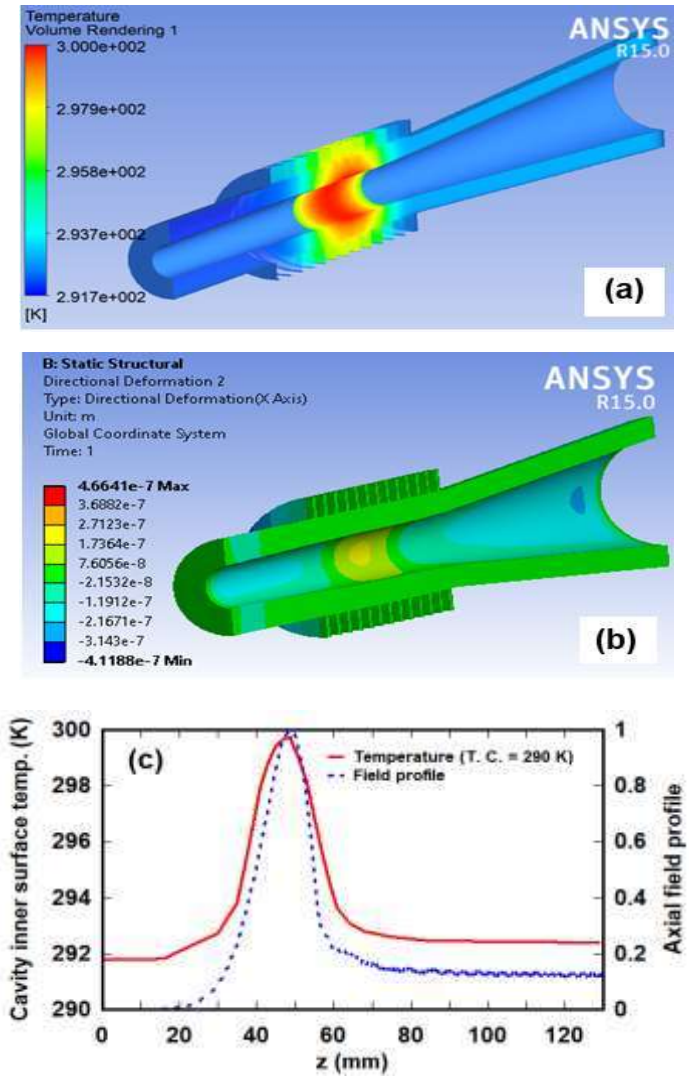

Figure 5.10 (a) Temperature distribution of cavity, (b) deformation distribution of cavity, and (c) temperature profile of the internal surface of the cavity and field profile of the cavity.

cavity with reduced conductivity as $\sigma = \sigma_{Cu}/2 = 2.9 \times 10^7$ S/ m. The same properties of OFHC–Cu given Chapter – 3 is reused in the present study. The heat flux (ohmic loss) in the cavity is calculated as ~335 kW /m^2 using the corresponding diffractive quality factor ~4900 [109], [114]. The heat flux is applied to the inner surface of the interaction cavity. As a result, the temperature in the cavity increases that causes the deformation in the cavity. To cool down the cavity, water is used as a coolant that flows between the grooves on the outer surface of the cavity. The temperature of the cavity is transferred from the inner surface to the outer surface by conduction and from the outer surface to

the coolant by convection. The width and height of the grooves are optimized as 1 mm and 2 mm, respectively. The thickness of the cavity is considered as 2 mm [112]. A total of 8.62 L /min of water passes through the channels (grooves) with a velocity of 3 m /s between the grooves. The heat transfer coefficient between the cavity surfaces and water is calculated as ~15500 W /m2–K using post-processing. To observe the radial deformation of the cavity, both ends of the multi-section cavity are fixed in the simulation. The temperatures on the inner and outer surfaces of the cavity are calculated as ~300 K and ~296 K, respectively, [Figure 5.10 (a)], while the coolant temperature (T. C.) is ~290 K. The temperature distribution at the inner surface of the cavity is in good agreement with the cavity field profile [Figure 5.10 (c)]. The radial deformation at the inner surface of the cavity (whose ends are fixed) is observed as ~0.32 μm [Figure 5.10 (b)]. The average temperature on the cavity's inner and outer surfaces is observed as ~293 K only when the coolant temperature is 283 K on the outer surface of the cavity. The observed deformation is negligible at the coolant temperature (T. C. = 283 K) in the RF cavity, which resonates at 260.05 GHz. As T. C. is 290 K, the resonant frequency is shifted to ~260.01 GHz from ~260.05 GHz (T. C. = 283 K). Therefore, the total frequency shift is obtained by ~40 MHz. This change in resonant frequency helps to increase the tuneable bandwidth by varying the coolant temperature.

5.5. Tuneability of Multi-Section Cavity Gyrotron

5.5.1 Magnetic Tuning Scheme

As the cyclotron angular frequency is directly proportional to the magnetic field, the magnetic tuning is preferred over electrical tuning. The $TE_{7,2}$ mode has mode

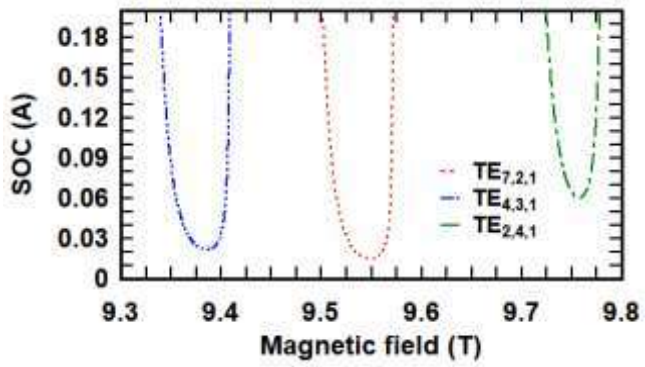

Figure 5.11 The start oscillation current of $TE_{7,2,1}$ mode with other competing modes field (for the beam parameters 15.5 kV, 100 mA, α = 1.12).

competition with the nearby modes $TE_{4,3}$ and $TE_{2,4}$. The possibility of mode competition can be reduced by choosing a proper beam radius and the magnetic field. The beam radius is chosen in such a way that $TE_{7,2,q}$ mode have maximum coupling to the electron beam and other competing modes like $TE_{4,3}$ and $TE_{2,4}$ have minimum coupling. For q = 1 in the present multi-section cavity, the start oscillation current (SOC) [Figure 5.11] of the operating mode and other competing modes are calculated. The Figure 5.11 predicts that a series of $TE_{7,2,q}$ modes can be excited in the span of 9.51 – 9.75 T. The SOC of the higher-order axial modes of $TE_{7,2,\,q}$ is also calculated, which is quite low [Figure 5.8], which helps to excite a series of axial modes of $TE_{7,2,\,q}$ in the RF cavity. In the present case, the axial mode number, q is varied from 1 to 9 with reference to the continuously varying magnetic field (B_o). In the present magnetic tuning, the magnetic field is varied from 9.51 T to 9.74 T, as a result, a series of axial modes of $TE_{7,2,q}$ (q = 1 – 9) are excited in the cavity with more than ~1.5 W output power [Figure 5.12 (a)]. A meagre and negligible power is observed in the competing $TE_{4,3}$ and $TE_{2,4}$ modes, as compared to operating $TE_{7,2}$ mode in the span of magnetic field, 9.51 T – 9.74 T. In the magnetic tuning process, the lowest $TE_{7,2,1}$ mode is found to be excited at 260.05 GHz and the highest $TE_{7,2,9}$ mode at 261.9 GHz with magnetic

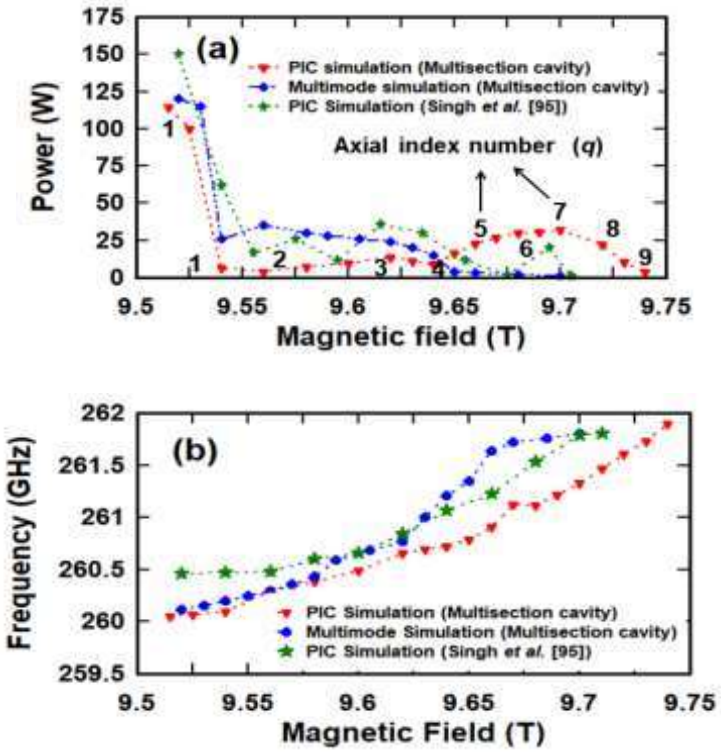

Figure 5.12 (a) Power Vs magnetic field, and (b) resonating frequency with the corresponding magnetic field (for the beam parameters 15.5 kV, 100 mA, α = 1.12, and velocity spread is 2 %).

fields of 9.51 T and 9.74 T, respectively. Therefore, the total tuneable bandwidth is obtained as ~1.85 GHz [Figure 5.12 (b)] in the magnetic tuning, which is ~0.55 GHz higher than the obtained tuneable bandwidth in a conventional cylindrical three-section gyrotron cavity [112]. Because the cavity field profile for q = 1 is shifted to the right (section L_4), where the radius of the cavity is slightly higher and for the higher-order axial mode $q \geq 6$, the cavity field profile is shifted to the left (section L_2), where the radius of the cavity is slightly smaller than the radius of the straight section (2.369 mm) of the three-section cavity. Therefore, the total increment of ~0.55 GHz in the tuneable bandwidth is the combined effect of the shifted frequency (~0.40 GHz) towards the lower frequency side due to section L_4 and the shifted frequency (~0.15 GHz) towards the higher frequency side due to section L_2. Further, the results obtained from the magnetic tuning have also been validated using a nonlinear time-dependent self-

consistent Multimode code, which shows a good agreement with the simulation results, as shown in Figures 5.12 (a) and 5.12 (b).

5.5.2 Thermal Tuning Scheme

Thermal tuning is another technique to further increase the tuneable bandwidth of gyrotrons by varying the coolant temperature. The cavity is operated at a single axial mode number (q = 1) in the thermal tuning. As the cavity temperature increases, the deformation of the cavity also increases, which in turn increases the radius of the cavity. Therefore, the cavity's cut-off frequency decreases as the cavity radius increases, resulting in a mismatch between the magnetic field and the operating frequency. The cavity's cut-off frequency is very close to the cyclotron angular frequency, and the applied magnetic field is very sensitive to the cyclotron angular frequency. Therefore, to synchronize the operating frequency with the magnetic field, the magnetic field is slightly reduced for the increased cavity radius. In the present thermal tuning, the coolant temperature is varied from 290 K to 365 K. The present multi-section RF cavity is observed at various coolant temperatures including 290 K, 300 K, 320 K, 340 K and 365 K that is lead to 300 K, 310 K, 330 K, 350 K and 375 K on the inner surface of the cavity, respectively. As a result, the deformation at the inner surface of the cavity is calculated as ~0.32 µm, ~0.72 µm, ~1.8 µm, ~2.75 µm, and ~4.2 µm, respectively. The cavity is again simulated by including the calculated deformation and obtained the RF output power as ~100 W, ~90 W, ~82 W, ~70 W, and ~65 W at the temperature ~290 K, ~300 K, ~320 K, ~340 K, and ~365 K, respectively [Figure 5.13 (a)]. The corresponding resonant frequency shift is observed as ~260.01 GHz, ~259.97 GHz, ~259.85 GHz, ~259.75 GHz, and ~259.58 GHz, respectively [Figure 5.13 (b)]. Therefore, the maximum thermal tuneable bandwidth is obtained as ~0.47 GHz with respect to the resonant frequency ~260.05 GHz for the coolant temperature ~283 K. In

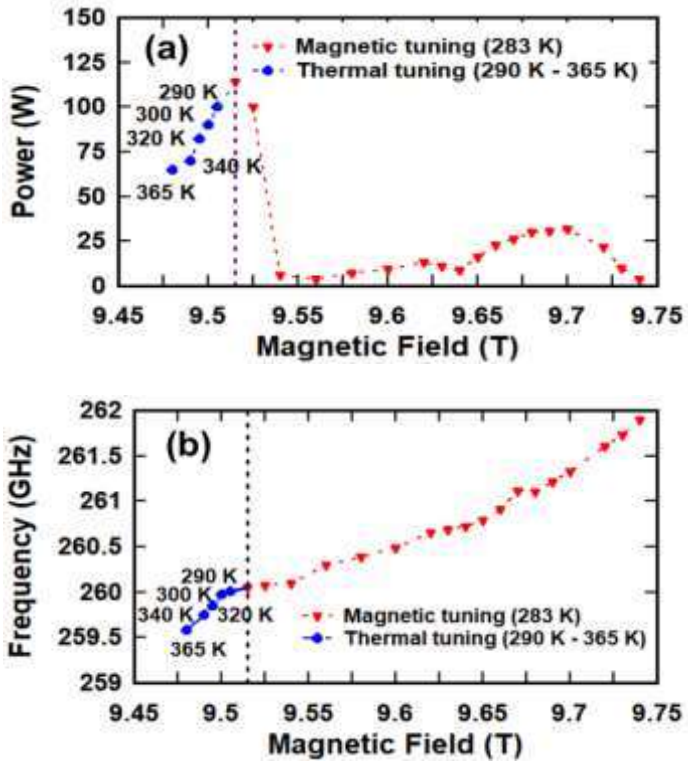

Figure 5.13 (a) Power Vs magnetic field, and (b) resonating frequency with the respective magnetic field at the respective coolant (water) temperature.

the present work, ~1.85 GHz and ~0.47 GHz tunable bands, is achieved using magnetic tuning and thermal tuning schemes. Since both tuning schemes are independent of each other, the tuneable bandwidth can be further increased by combining both tuneable schemes. Therefore, the total tuneable bandwidth is obtained as ~2.32 GHz, which is ~25.40 % higher than the tuneable bandwidth achieved by the magnetic tuning scheme.

5.6 Discussion on Fabrication Aspects of the Cavity

As given in Table – 5.1, the difference between the radii at both ends of section L_2, L_3 and L_4 are ~4.19 µm, ~2.68 µm and ~2.09 µm, respectively, which is much higher than 0.2 µm. The effect of imperfection in manufacturing is detailed in [136]. A gyrotron cavity was successfully designed and fabricated with the precision of ~0.2 µm [71]. The minimum precision is required in the deviation of the radius is given by [137],

$$\Delta R(\mu m) < \frac{1}{16} L(mm) \chi_{m,n} \left(\frac{\beta_{\perp o}^2}{\beta_{zo}} \right)^3 \tag{5.3}$$

From (5.5), for the beam voltage of 15.5 kV, velocity ratio α = 1.12 (≤ 1.8), with the cavity length L_3 = 22 mm and slightly taper angle $\theta_3 = 0.007^0$ operating in $TE_{7,2}$ mode, the precision ΔR is calculated as ~0.145 μm. The fabrication of the cavity with such accuracy is possible but quite challenging. The minimum exact ΔR can be increased by increasing the cavity length, Eigenmode number $(\chi_{m,n})$, and velocity ratio α. Therefore, to realize the cavity with a precision greater than ~0.2 μm, the velocity ratio, α must be greater than ~1.21 for the present multi-section cavity. In the present work, the velocity ratio α is considered to be ~ 1.12, due to an unbiased comparison with the three-section cavity based gyrotron discussed in Chapetr – 3 [112]. Since the velocity ratio in the beam parameters can be taken up to ≤ 1.8 [74]. However, the fabrication with an accuracy of up to ~ 0.1 μm is possible with the help of the electroforming technique [138]. Therefore, it will not be challenging to fabricate the present cavity using an Electroforming technique with an accuracy of ~ 0.2 μm.

5.7 Conclusion

In the present chapter, a multi-section RF interaction cavity for millimeter-wave gyrotron has been designed and studied for its diffractive quality factor and resonanting frequency using the minimization method. The use of a multi-section RF cavity with slightly up-tapered sections shift the field profile from the lower frequency to higher frequency sides that helps to vary the axial index of the operating mode. The present multi-section cavity gyrotron has been simulated using the "CST Particle Studio" code to observe the Multimode beam-wave interaction characteristics and obtain a continuous wave output power ~114 W $TE_{7,2,1}$ mode at 260.05 GHz. Further, to increase

the present gyrotron's tuneability, both magnetic and thermal tuning schemes have been adapted. The present gyrotron's magnetic tuning swept a range of ~1.85 GHz while varying the axial mode index, q = 1 to 9, and thermal tuning added ~0.47 GHz. Therefore, the present multi-section RF cavity has enhanced the tuning bandwidth of gyrotron to ~2.32 GHz by thermal and magnetic tuning schemes. It is hoped that the tuneable bandwidth (~2.32 GHz) obtained from the present millimeter wave gyrotron will prove to be quite useful for 400 MHz NMR spectrometer in DNP / NMR experiments.